Soft Matter

Accepted Manuscript

ROYAL SOCIETY OF CHEMISTRY

www.rsc.org/softmatter

Soft Matter

RSCPublishing

ARTICLE

Phase behaviour of PMMA-*b*-PHEMA with solvents methanol and THF: Modeling and comparison to experiment

Cite this: DOI: 10.1039/x0xx00000x

Received 00th January 2014,
Accepted 00th January 2014

DOI: 10.1039/x0xx00000x

www.rsc.org/

P. Padmanabhan[a], M. Chavis[b], C. K. Ober[b] and F. A. Escobedo*[a]

Self-consistent field theory is used to model the self-assembly of a symmetric PMMA-*block*-PHEMA in the presence of two solvents, methanol and tetrahydrofuran (THF). The model predictions are compared to our experimental results of vapour-solvent annealing of thin polymer films, where the sequence of cylinder to gyroid (or micelles) to lamellar phases was found upon increasing the methanol:THF ratio and for particular extents of film swelling. The Hansen solubility parameters are used to estimate the Flory-Huggins interaction parameters (χ) needed in the theoretical model. However, because enacting the experimental range of high χN values is computationally prohibitive, the use of moderate χN values is compensated by employing larger values of the solvent-to-polymer size ratio (α). This approach is validated by showing that the predicted phase diagrams exhibit qualitatively similar trends whether χN or α is increased. Using such an approach, the theory predicts a cylinder to gyroid to lamellar transition on increasing the THF:methanol ratio, a trend consistent with that observed in the experiments.

[a] School of Chemical and Biomolecular Engineering, Cornell University, Ithaca, NY 14853.
[b] Department of Materials Science and Engineering, Cornell University, Ithaca, NY 14853.
* Corresponding author: fe13@cornell.edu

1 Introduction

The self-assembly of block copolymers has long been used for the synthesis of materials for a variety of applications like photovoltaic devices[1], catalysts[2], enantiomer separation devices[3] and nanolithography[4]. Controlling the morphology and tailoring its feature size for a specific application are challenging because in block copolymer melts, these are primarily determined by two key parameters: interaction strength (Flory-Huggins parameter χ times the degree of polymerization N) and volume fraction f of one of the blocks. Furthermore, after the copolymer has been synthesized (fixed f and N), the only handle available to tune the morphology is temperature (which is inversely related to χ). However, morphology control via temperature has some drawbacks since temperature annealing can access multiple phases only near the order-disorder transition (ODT), and for many polymer chemistries of interest the ODT may be high enough to cause polymer degradation. Instead, solvent annealing of the block copolymer with varying solvent concentrations has been successfully used to tune the morphology[5-10]. Furthermore, in thin films, solvent annealing neutralizes the surface energy of the air interface allowing further morphological control[11,12]. While using a single solvent does provide some tunability, finding the ideal solvent quality and degree of selectivity (for either block at the temperature of interest) can be restrictive if only one among a handful of existing solvents is to be considered. This limitation is readily removed by using a mixture of two (or more) solvents, so that, e.g., varying the composition of the solvent can allow tuning solvent quality at a fixed temperature. This approach then provides multiple handles to control morphology and feature size: amount of solvent(s) in the mixture, ratio of solvent quantities, and selectivity (determined by chemistry and temperature). Indeed, solvent vapour annealing has been shown to allow access to structures that are unattainable through thermal annealing[9,10]. Recently, the two-solvent approach was used to successfully demonstrate control over the lamellar width of sub-20 nm lamellar domains[12].

Self-consistent field theory (SCFT) has shown considerable success in modelling the self-assembly of block copolymer melts at low to intermediate values of χN. In particular, it predicts the stability of the gyroid phase up to $\chi N=100$[8], a prediction that has been verified in experiments. Another advantage of SCFT is that it can be easily extended to include solvents. However, the SCFT equations quickly get computationally intensive as χN is increased due to the increase in the number of basis sets needed for numerical convergence, thus limiting the range of parameters that can be studied. Keeping that limitation in mind, we adopted this well-established theoretical framework for the present study.

Several theoretical studies have used SCFT to map out regions of the multidimensional phase diagram of block copolymers upon the addition of solvents. A phase selective solvent lowers the overall χN[10] by acting as a plasticizer and swelling the polymer. It also alters the effective *f* value by inducing preferential swelling of one block domain. Several early studies focused on the regime where the solvents were dilute and neutral, thus, $\chi_{eff} = \varphi_{polymer}\chi$[13,14] and there was no preferential swelling. In such cases the ODT decreases monotonically as more solvent is added[14]. For a single selective solvent, the phase diagram shifts toward the selective phase[15], much like the shift of the phase diagram toward the block type having a larger Kuhn length. The solvent size is typically much smaller (a few angstroms) than that of the block copolymer (tens of nanometres), and since the morphologies have features sizes on the order of the block length, the solvent is approximated as a structureless particle with a finite size (with ratio of solvent size to polymer size = α). The smallness of α has been found to lead to a fairly uniform spatial distribution of the solvent except near the interfaces[16].

The vast majority of the work with SCFT has focused on the effect of solvent on the formation of lamellar, cylindrical, and micellar phases[14,16-18]. In this work we studied the phase behaviour of poly(methyl methacrylate)-*block*-poly(2-hydroxyethyl methacrylate) (PMMA-*block*-PHEMA) with tetrahydrofuran (THF) and methanol by using both solvent-annealing experiments and SCFT. Particularly, we are interested in exploring the thermodynamic stability of the gyroid phase since, unlike other phases commonly found in block copolymers, it is bicontinuous which means that the two block domains interweave uninterrupted in all directions. This leads to nanostructures with enhanced mechanical stability (even if one of the block domains is etched away) and transport properties (for thermal or electrical conduction) that are the same regardless of sample spatial orientation; these qualities make the gyroid phase appealing for such potential applications as active porous matrices for solar cells[19], batteries, and separation devices. We find that the gyroid phase is observed in our experiments at conditions which are fairly consistent with those where SCFT predicts its stability.

The rest of the article is organized as follows. In Section 2, the experimental results are briefly described. In Sections 3 and 4 the theory and the estimation of model parameters used by the theory are presented. In Section 5 the modelling results are expounded and discussed. Finally, the main conclusions are summarized.

2 Experimental results

The block copolymer used was a 50:50 mass ratio PMMA-*block*-PHEMA, of molecular weight 40 kDa and polydispersity 1.08. The PMMA-*block*-PHEMA chemistry selected is appealing for nanolithography because it allows one to harness both a top-down approach[20] by virtue of one of the blocks being photosensitive, as well as a bottom-up approach by exploiting the self-assembly of the diblock chains into specific nano-segregated morphologies. The experiments were conducted at room temperature which is well below the glass transition temperature of the two blocks in the polymer. Upon thermal annealing, the pure copolymer forms a lamellar phase with about a 40nm spacing.

Table 1 summarizes the results from experiments. A detailed explanation of the methods and their application is the topic of a separate article[21]. In brief, the copolymer was spin-coated to a thin film. Due to rapid processing conditions, the as-spun thin film was disordered. It was then exposed to vapour with the solvent mixture composition of interest. The solvent-annealing time and the resulting morphologies are listed in Table 1. The swelling ratio is calculated as the ratio of film thickness after and before exposure to solvent. The resulting morphologies were characterized by the analysis of both AFM images and *in-situ* GISAXS measurements; representative AFM images are shown in Figure 1. In all cases, exposure of the film after solvent annealing caused rapid evaporation of the solvent preserving the same morphologies although with uniaxial shrinking.

For the two extreme compositions, a lying cylinder morphology (finger-like AFM pattern) is obtained at the 80:20 methanol:THF ratio, whereas a lying lamellae is observed at the 20:80 methanol:THF ratio. At the 50:50 methanol:THF ratio, a gyroid morphology (pin-wheel like AFM pattern) is observed at long annealing times but spherical micelles are seen at short annealing times. Given that the latter difference is observed for identical swelling ratio, it suggests that kinetic effects were significant, or external conditions were not identical (or varied slightly over exposure time), or both. It would hence be helpful to use a theoretical framework like SCFT to try to outline the regions of thermodynamic stability for the different phases observed experimentally. A more detailed description of the experiments and results (including GISAXS spectra) is given in Ref. 21.

Composition (Vol %) (Methanol/THF)	Film thickness	Swelling ratio	Time (seconds)	Resulting morphology
Pure copolymer	145 nm	1.00		Disordered (no annealing)
80/20	440 nm	3.03	6300	Lying cylinders
50/50	368 nm	2.53	6300	Spherical micelles
50/50	368 nm	2.53	20700	Gyroid
20/80	460 nm	3.17	6300	Lying lamellae

Table 1: Experimental parameters and results.

Soft Matter RSCPublishing

ARTICLE

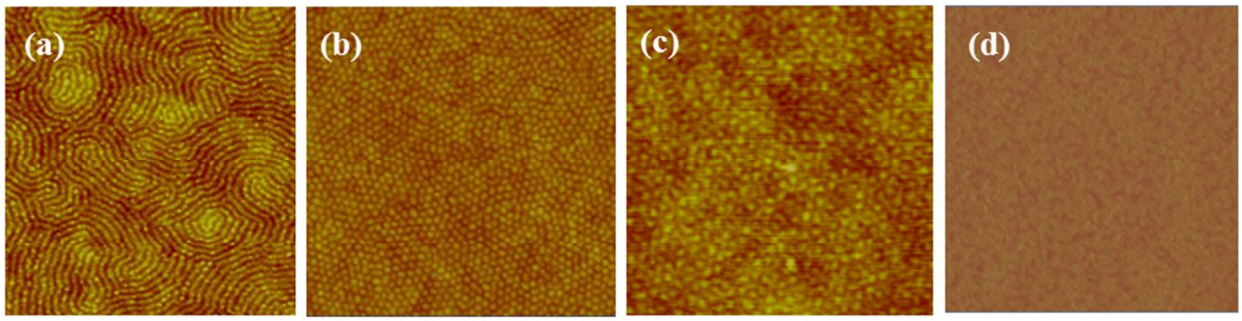

Figure 1: AFM images of solvent-annealed polymer morphologies listed in Table 1. (a) Lying cylinders (b) Spherical micelles (c) Gyroid (d) Lying lamellae.

3 Theory

Self-consistent theory[13,15,22,23] treats the solvent as a structureless particle, the polymer as a continuous Gaussian chain and the entire system to be incompressible. For our system, there are four chemical 'species' denoted by subscript *i* in the system – two monomers and two solvents, and three components (subscript *c*)– one block copolymer and two solvents. The degree of polymerization is *N* and the fraction of PMMA in the copolymer is *f*. The overall volume fraction of copolymer in solution is φ_P and those of methanol and THF are φ_M and φ_T, respectively; local densities are denoted by ϕ_c. The ratio of solvent size of methanol and THF to polymer size are respectively α_M and α_T. In SCFT, particles are in effective fields $\{\omega_i(\mathbf{r}); i=1,4\}$. For each kind of species *i* in the system,

$$\omega_i(\boldsymbol{r}) = \sum_{j\neq i} \chi_{ij} N \phi_j(\boldsymbol{r}) + \xi(\boldsymbol{r}) \qquad (1)$$

where $\xi(\boldsymbol{r})$ is a Lagrange multiplier to enforce the incompressibility constraint on dimensionless local concentrations, $\sum_i \phi_i(\boldsymbol{r}) = 1$. The polymers are parameterized by a contour variable $0<t<1$. $q_P(r,t)$ is the chain propagator of the 0-t^{th} region in a polymer chain at location **r** and obeys the diffusion equation:

$$\frac{\partial q_P(\boldsymbol{r},t)}{\partial t} = \begin{cases} \frac{Nb_A^2}{6}\nabla^2 q_P(\boldsymbol{r},t) - w_A(\boldsymbol{r}) q_P(\boldsymbol{r},t), & 0 < t < f \\ \frac{Nb_B^2}{6}\nabla^2 q_P(\boldsymbol{r},t) - w_B(\boldsymbol{r}) q_P(\boldsymbol{r},t), & f < t < 1 \end{cases}, \qquad (2)$$

with $q_P(\boldsymbol{r},0) = 1$. And its complimentary from t+1th to N^{th} region in the polymer chain is given by

$$\frac{\partial q_P{}^+(\boldsymbol{r},t)}{\partial t} = \begin{cases} w_A(\boldsymbol{r}) q_P{}^+(\boldsymbol{r},t) - \frac{Nb_A^2}{6}\nabla^2 q_P{}^+(\boldsymbol{r},t), & 0 < t < f \\ w_B(\boldsymbol{r}) q_P{}^+(\boldsymbol{r},t) - \frac{Nb_B^2}{6}\nabla^2 q_P{}^+(\boldsymbol{r},t), & f < t < 1 \end{cases}, \qquad (3)$$

with $q_P{}^+(\boldsymbol{r},1) = 1$. Under the assumption that the solvent is structureless, the diffusion equation for its propagator reduces to

$$\frac{\partial q_S(\boldsymbol{r},t)}{\partial t} = -w_s(\boldsymbol{r}) q_s(\boldsymbol{r},t) \qquad (4)$$

The partition function of the polymer is given by $Q_p = \frac{1}{V}\int d\boldsymbol{r}\, q_p(\boldsymbol{r},1)$, and for each solvent *S* is $Q_s = \frac{1}{V}\int dr\, q_s(r,\alpha) = \frac{1}{V}\int dr\, exp(-\alpha_s \omega_s(\boldsymbol{r}))$. The local concentrations for the polymer are $\phi_P(r) = \frac{\varphi_P}{V}\int_P dt\, q_P(r,t) q_P{}^+(r,1-t)$ and for the solvents are $\phi_s(r) = \frac{\varphi_s}{V}\exp(-\alpha_s\omega_s(\boldsymbol{r}))$.

The free energy per molecule becomes

$$\frac{F}{kT} = -\sum_c \frac{\varphi_c}{\alpha_c}\ln\left(\frac{\alpha_c Q_c}{\varphi_c}\right) - \int d\boldsymbol{r}\{\sum_c \omega_c(\boldsymbol{r})\phi_c(\boldsymbol{r})\} \qquad (5)$$

These SCFT equations are solved using the Polymer Self Consistent Field (PSCF) code[24] which requires a good initial guess for convergence. The ternary phase diagram at a given χN and α was systematically mapped out using the solution from a nearby point for quick convergence. The starting point was chosen as a PMMA-*block*-PHEMA copolymer melt. Methanol was subsequently added (traversing along one axis in composition space), and finally THF was added to span the rest of the phase diagram. Initial simulations were run using only the lamellar and cylindrical phases to quickly search the parameter space; the parameters were then tweaked to produce a cylinder phase in methanol-rich regions and a lamellar phase in THF-rich regions. It was also checked that the choice of traversal of axis (methanol first and THF second, or vice versa) did not affect the free energy calculation.

The number of basis sets N_b required for convergence of the numerical simulation increases rapidly as the Flory-Huggins parameter increases; this is because the block interfaces become sharper and more basis functions are needed to describe the domain shapes. This large number of basis sets rapidly escalates the simulation time needed, especially as the dimension of the morphology increases (lamellae are one dimensional, cylinders are two-dimensional, while gyroid and spherical micelles are three-dimensional). The inclusion of three-dimensional phases severely limits the range of Flory-Huggins parameter accessible by the theory.

4 Calculation of Parameters and Modelling Details

The input parameters in SCFT include chain architecture, volume fraction of the chain, Flory-Huggins interaction parameters and solvent size. Table 2 gives details of the chain architecture.

	Molecular weight of monomer (g/mol)	Degree of polymerization N_A	Kuhn length (nm)	Mole fraction, x	Volume fraction, f^a
PMMA	100.12[25]	200	1.7[26]	0.57	0.52
PHEMA	130.14[25]	154	1.03[27]	0.43	0.48

Table 2: Polymer parameters studied

Based on the monomer volume, PMMA has approximately 3 monomers per Kuhn segment while PHEMA has about two. Since a Kuhn segment is composed of about two-three monomers, the effective degree of polymerization N to be used in the SCFT model is 200/3 + 154/2 ≈144. The Flory-Huggins parameter captures the enthalpic chemical interaction between every pair of species. A positive value indicates repulsive energy whereas a negative value indicates attractive energy. Various empirical formulae exist in the literature to estimate the Flory-Huggins parameters for polymer-polymer, solvent-solvent and polymer-solvent interactions. In this work, we used the relation between Flory-Huggins parameter and solubilities of the constituents which follows the general principle that 'like solvates like'. It is estimated by the relation[28] $\chi_{12} = \frac{V_{ref}}{RT}(\delta_1 - \delta_2)^2$ where χ_{12} is the Flory-Huggins parameter, V_{ref} is reference volume and δ_i is the Hildebrand solubility parameter (for non-polar species) of the constituent i. Note that with this formalism the Flory-Huggins parameter cannot be negative and it is inversely proportional to temperature, allowing us to use scaled parameters. For our system, we have used the set of three Hansen solubility parameters[29] in order to incorporate polar and hydrogen bonding effects into the single Flory-Huggins parameter with the relation

$$\chi_{12} = \frac{V_{ref}}{RT}\left[\left(\delta_{1,d} - \delta_{2,d}\right)^2 + \left(\delta_{1,p} - \delta_{2,p}\right)^2 + \left(\delta_{1,h} - \delta_{2,h}\right)^2\right]. \quad (6)$$

The Hansen solubility parameters have a contribution from dispersive (subscript d), polar (p) and hydrogen bonding (h) forces. The solubility parameters for the polymers vary considerably across the literature based on estimation technique, and, for this current work, these are estimated from group contribution methods[30]. The solubility parameters for the solvents are from standard tables[31]. Table 3 lists the values of solubility parameters used and Table 4 lists the values of Flory-Huggins interaction parameters at 298 K scaled by $\chi_{PMMA-PHEMA}$≈2.08. Thus, χN would be 300 for the block copolymer.

It can be inferred from Table 3 that methanol is a poor solvent, with its interaction with PHEMA being more unfavourable than that of PMMA with PHEMA. On the other hand, TFH and PMMA have almost identical interaction parameters; the key difference between them being that THF is a structureless solvent while PMMA is a chain that has conformational degrees of freedom.

	$V_{monomer/solvent}$	δ_d	δ_p	δ_h
	(cm^3/mol)	($J^{1/2}$ $cm^{3/2}$)		
PMMA (group contribution)	85	17.66	5.76	7.82
PHEMA (group contribution)	107	17.3	6.51	15.57
THF	81.7	16.8	5.7	8.0
Methanol	40.7	15.1	12.3	22.43

Table 3: Solubility parameters used in the estimation of Flory-Huggins interaction parameters[30,31]

$\chi/\chi_{PMMA-PHEMA}$	PMMA	PHEMA	THF	Methanol
PMMA	0	1	0.01	4.31
PHEMA	1	0	0.96	1.4
THF	0.01	0.96	0	4.18
Methanol	4.31	1.4	4.18	0

Table 4: Flory-Huggins parameters normalized by $\chi_{PMMA-PHEMA}$.

Test runs and adjusting χN and α

For computational expediency, some departures from experimental conditions were introduced. The experimental system consists of a thin film of thickness a few hundred nanometres (see Table 1), which is many times the unit cell of any morphology of interest. The films were cast on native silicon oxide whose polarity imparts some affinity for the polar groups in both PMMA and PHEMA segments and hence one would expect both polymers to have similar substrate wetting properties (the analysis of "as spun" films of the pure diblock copolymer revealed domains with no long-range order nor preferential orientation with respect to the interfaces). While solvent

annealing tends to neutralize the surface energy of the air interface, its effect on substrate wetting is more difficult to assess. It is expected that any preferential substrate-polymer interaction will primarily affect the orientation of block domains (relative to the surface) rather than the type of morphology (phase) that it forms. However, if a strong substrate preference for one block were to occur then the tendency to form, e.g., a lying lamellar phase could be enhanced. For our study, we will neglect interfacial effects and focus only on bulk properties, assuming that both solvents are absorbed in the bulk phase. The swelling factor is thus the inverse of the average block copolymer volume fraction. The Flory-Huggins parameters in Table 4 only provide a qualitative picture of the interactions because errors in estimation of solubility parameters propagate and are magnified when using Eq. (6). Since the experiments showed a gyroid phase between cylinder and lamellar phases as the solvent ratio was varied, we perform initial tests probing the stability of lamellar and cylinder phases for a range of conditions. The tests indicated that either a larger Flory-Huggins parameter disparity between methanol and PMMA, or a larger solvent size than experimental conditions is required to achieve stable cylinder and lamellar phases in the range of compositions of interest.

Since the simulation becomes costly on increasing the Flory-Huggins parameter disparity, we only use the ratio fixed by the Hansen solubility parameters. The scaled Flory-Huggins parameters in Table 4 reflect the actual chemistry of the copolymer and solvents, and we will refer to $\chi_{PMMA\text{-}PHEMA}$ as χ henceforth. The other parameters are scaled according to Table 4. Furthermore, the range of χ explored is limited to $20 \leq \chi N \leq 40$ (and 50 in a special case) due to computational expediency, which is much smaller than the value of 300 that was estimated in the previous section. The contribution to the mixing free energy in Equation (5) increases inversely as the size of solvent is reduced. Indeed at very low solvent size ratio, the disordered phase is favoured and a very high value results in a breakdown of the assumption of the solvent being structureless in comparison to the block copolymer. In order to compensate for the relatively low value of χN that we can practically adopt, we increase α but stay within a range of values that has been used in previous SCFT studies of block copolymers with solvents[14-18]. Specifically, we performed simulations with $\alpha_{methanol}$=0.002 (closest to the experimental value), 0.005 and 0.01. α_{THF} is scaled accordingly. A similar approach was used in a previous SCFT study wherein a lower χN and solvent molecules with the same size of statistical monomer unit (α~0.005) were used to model the lamellar to cylinder transition observed in experiments of PS-PMMA with two solvents[32]. Henceforth, we will only refer to the parameter $\alpha_{methanol}$ and drop the subscript. The phases studied are disordered (homogeneous), lamellar, cylindrical and gyroid phases. The BCC spherical micellar phase has been included only in a special case due to the difficulty in attaining convergence for this phase with a 50:50 block copolymer. Free energies of various phases under study are compared and the one with the lowest free energy is identified as the stable phase (the normalized free energies are calculated to within 10^{-4}). In all cases studied, we do not find multiphase coexistence (See Appendix 1 for more details).

5 Modelling Results

Three dimensional ternary phase diagrams for the PMMA-*block*-PHEMA + methanol + THF system are shown in Figure 2 for different choices of χN and α parameters. The vertex on the right in each ternary diagram corresponds to pure DBC and thus a swelling factor of 1. The vertex on the left is pure methanol and the vertex on the far back is pure THF. The experimental observations are overlaid using dashed lines/shaded regions for visual comparison. Since the exact partitioning of the solvents into the experimental polymer film is unknown, we assume that the solvent compositions match those of the annealing vapour phase. The vertical axis at a swelling factor=φ_{DBC}=1 corresponds to the phase diagram of the pure diblock copolymer. Since we have a near 50-50 volume ratio and we are above χN_{ODT} (~10.5) for a melt, we find a stable lamellar phase at this axis for all values of χN in Figures 2a through 2c.

For α=0.002 (Figure 2a), a transition to the disordered phase takes place as the swelling factor is increased. Since $\chi_{methanol\text{-}polymer} > \chi_{THF\text{-}polymer}$, the THF-rich mixture undergoes an ODT at lower solvent concentrations than the methanol-rich mixture at a given swelling factor and χN. As χN is increased, the ODT occurs at higher solvent concentration (and thus, higher swelling factor). Interestingly, the transition to the disordered phase is different between the methanol-rich and the THF-rich regions. The THF-rich region undergoes a lamellar to disordered transition, while in the methanol-rich region, the disordered phase may be approached via the cylinder, gyroid or lamellar phases depending on the χN and swelling factor. As justified in the previous section, we also explore the phase diagram for higher solvent sizes.

The phase diagram for α=0.005 is shown in Figure 2b. At χN=20, the stable phases are the lamellar and disordered phases. At χN=30 and higher, the methanol-rich axis transitions from lamellar to gyroid to cylinder phase as the swelling factor increases. At a given swelling factor, depending on the starting point at the methanol-rich plane, a cylinder to gyroid to lamellar transition occurs as the THF fraction in the solvent mixture is increased. Furthermore, the gyroid region of stability is widest for χN=30 and gets narrower as χN is increased. The phase diagram for α=0.01 in Figure 2c is qualitatively similar to that of Figure 2b except for an apparent shift upward of χN as α is increased; e.g., the diagram for χN = 40, α=0.005 looks most similar to that for χN = 30, α=0.01. Figure 3 illustrates this by showing the effect on increasing α at constant χN which looks qualitatively similar to Figure 2b. Thus, in this region of phase space explored, we have an *effective* χ parameter that increases monotonically with φ and α.

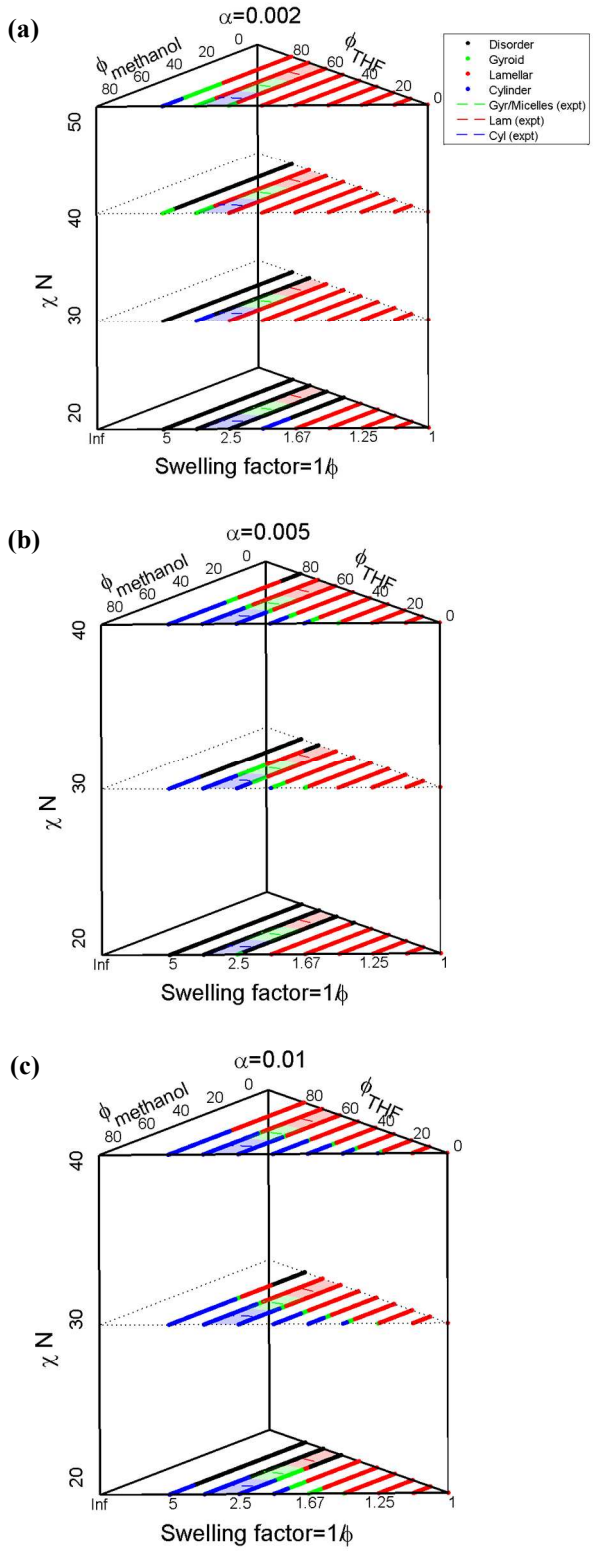

Figure 2: Ternary phase diagram for (a) α = 0.002, (b) α = 0.005 and (c) α = 0.01. The dashed line and shaded region represent the region of swelling ratios and solvent compositions studied by the experiments.

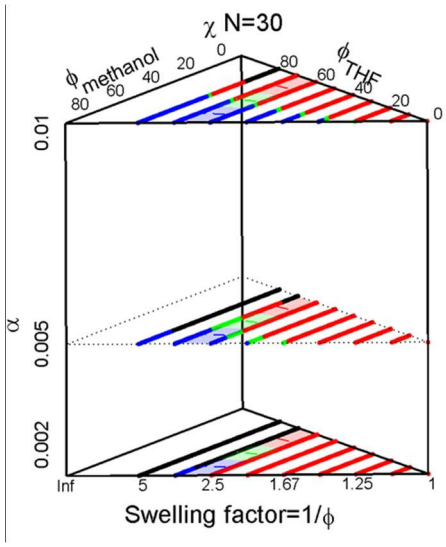

Figure 3: Phase diagram at constant χN for increasing α.

Approximate comparison with experiment

For a specific case of parameters (χN=30, α=0.01), we have also included the BCC spherical micellar phase and double diamond phase in the calculations for obtaining the phase diagram (plotted in Figure 4). Here, the diamond phase is not stable in any region of the phase diagram while spherical micelles replace part of the phase region where cylinders are stable in Figure 1. The spherical micelles become stable near the ODT and the methanol-rich region. Comparing Figure 4 with Figure 3, the progression of phases is much the same upon including the spherical phase (lamellar to gyroid to cylinder to spherical micelles) and is consistent with the effect of reduced χ_{eff} on increasing swelling. Consistent with experimental data, the theory predicts the presence of cylinder and lamellar phases at the 80:20 and 20:80 methanol:THF ratios respectively.

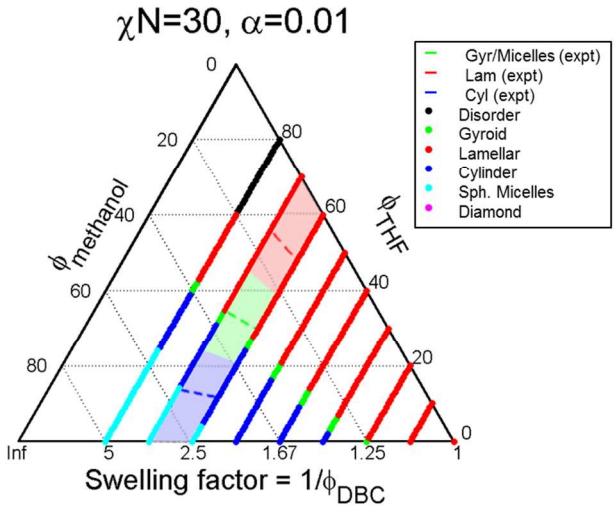

Figure 4: Phase diagram including spherical micelles and double diamond in the calculation. Minority phase = PMMA. α=0.01.

From the theory, near the 50:50 methanol:THF region, one would expect a transition from micelle to gyroid upon increasing the methanol:THF ratio to occur via an intermediate cylinder phase. In the experiments, this intermediate phase was not seen. One reason for this discrepancy could be that the experimental solvent composition in the polymer film is not necessarily identical to that of the imposed vapour phase composition due to partitioning of components among the vapour and film phases (and that these compositions may have slightly changed during a long annealing period). Even in the simplest case of a binary methanol and THF mixture, the compositions of the coexisting vapour and liquid phases would not be identical[33]. A second possible reason for the absence of the cylinder phase in experiments for this case could be slow kinetics of the gyroid to cylinder transition. Previous studies in the literature of block copolymer melts have shown epitaxial pathways of instability for χN=20 and lower[34-37]. This region of metastability of the gyroid phase for a pure block copolymer melt was shown to extend well into the cylinder phase, close to the cylinder to micelle transition[37]. Furthermore, the free energy barrier for gyroid to cylinder increases with χN[35]. This scenario seems likely given that the morphology at 50:50 solvent ratio in experiments nucleates from a disordered film and evolves over time.

Density distributions across the microstructure

We also investigated the spatial distribution of densities normalized by the overall volume fraction of the various components. The densities of the polymer blocks usually vary widely between zero and its maximum value while the solvents, being much smaller, have a more uniform distribution with little variations of density from its average, by less than 10% for low values of α. As the swelling factor is increased, the width of the interface increases and the relative density deviations about the mean are suppressed, eventually leading to a disordered phase (not shown). THF and methanol behave slightly differently. THF accumulates at the PMMA-PHEMA interface, whereas methanol prefers the center of the PHEMA domain. Due to the high selectivity of methanol, increasing the ratio of methanol to THF increases the relative width of the PHEMA domain for all phases under study (not shown).

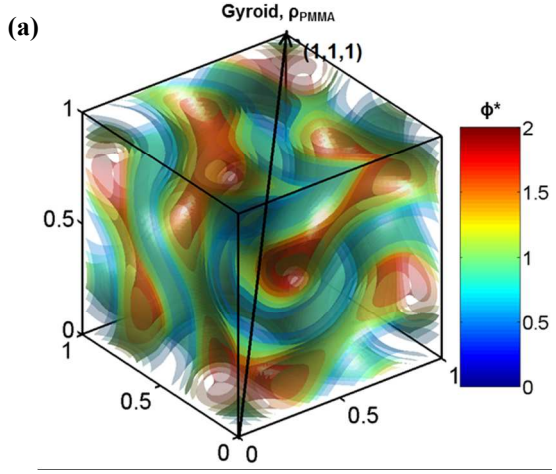

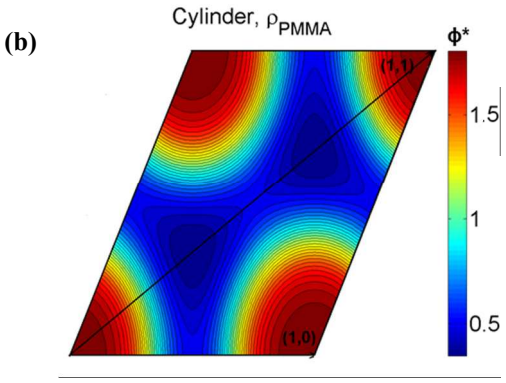

Figure 5: Isosurfaces of normalized density of PMMA for (a) the gyroid phase, and (b) the cylinder phase.

On the other hand, increasing the ratio of THF to methanol results in a higher accumulation of THF at the interface, with no significant change in the relative width of the PMMA domain. Figures 5a and 4b show density isosurfaces for gyroid and cylinder phases respectively, obtained at conditions χN=30, α=0.05, swelling factor = 3.3 with 80:20 methanol:THF. Figure 6 shows a comparison of density distributions for different phases as solvent size increases. For the sake of clarity, density distributions for multidimensional phases in Figure 6 are shown along the vectors noted in Figures 5a and 5b. For χN=30, swelling factor of 3.33 and 80:20 methanol:THF, as α is increased from 0.002 to 0.01, the stable phases are disordered, gyroid and cylinder (see also Fig. 3a). As α is increased, methanol exhibits a stronger preference for the core of the PHEMA-rich domains. For α=0.005 the positive (and negative) relative deviations in density from the average is about 20%, whereas for α=0.01 this deviation is as high as 50% In this case, even PHEMA is repelled from the core of the majority domain and is concentrated near the interface.

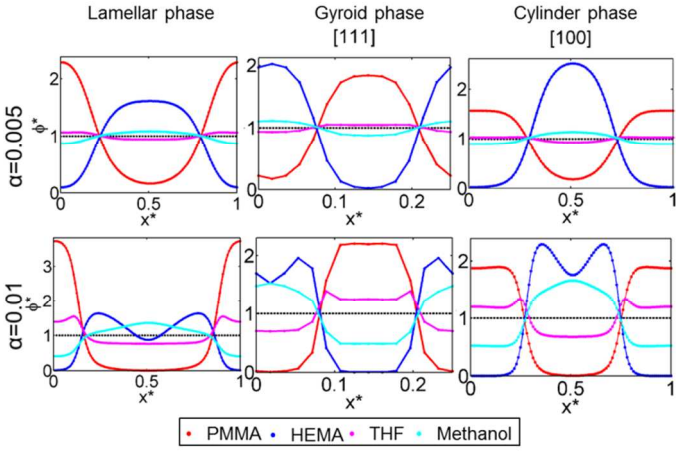

Figure 6: Effect of increasing α on the density distributions of different components. Morphologies relevant to χN=30, swelling factor = 3.3 with 80:20 methanol:THF. The lowest value of α is not shown here (disordered phase produces a flat distribution of densities).

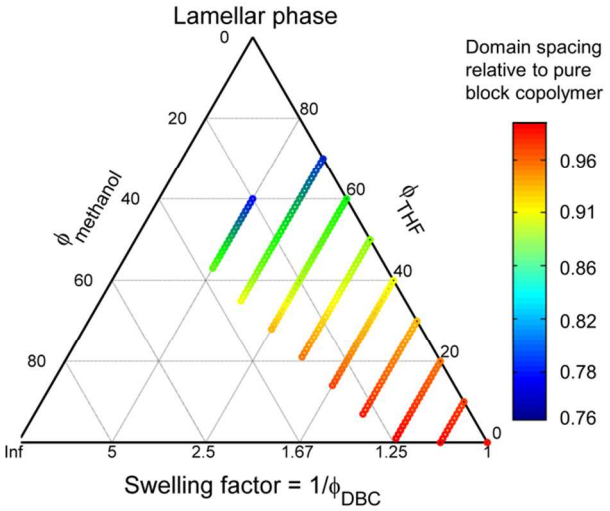

Figure 7: Effect of solvent addition on domain spacing for the lamellar phase at χN=30, α=0.01.

The aforementioned effect of methanol exclusion from the centers of PHEMA domain is not seen when increasing χN at fixed α (Figure B in appendix 2), at least within the range of χN explored. This suggests that although the "macroscopic" phase diagrams look qualitatively the same on either increasing χN or increasing α, due to changes in the "microscopic" behavior of solvent distribution, these scenarios are certainly not equivalent.

From SCFT, one can also get domain sizes of various morphologies. Figure 7 shows the region of phase diagram where the lamellar phase is stable, color coded by the domain spacing (normalized by that of the pure block copolymer). As swelling increases, the domain size decreases, an effect that is minimal in the methanol-rich region and becomes larger as the THF:methanol ratio is increased. The largest spacing reduction we observe (26%) is more significant than that (9%) reported in Ref. 12 (for a different system), likely a reflection of the larger swelling ratios we explore. A simplistic explanation of this spacing-reduction is that when the domains are swollen by a good solvent (like THF), the inter-block interfacial tension decreases and its area increases; hence the polymer chain "brushes" that stick out from opposite sides can interpenetrate more. Domain size reduction and enlargement can occur for other phases (results not shown). Figure 7 further illustrates (as in Ref. 12) that solvent annealing may be an effective technique for decreasing the domain size (appealing for lithographic applications), and particularly in our case, for the lamellar phase which occurs for THF-rich conditions.

Conclusions

We have studied the phase behaviour of 50:50 PMMA-*b*-PHEMA with methanol and THF using both experiments and an approximate model via SCFT. Experiments were limited to 3 solvent compositions (and for specific swelling ratios) revealed the formation of different phases including the gyroid phase. Given the uncertainties and challenges associated with exactly matching experimental systems with model parameters, we used SCFT to investigate the dependence of the phase diagram for intermediate values of Flory-Huggins' interaction parameters and a range of solvent sizes. Starting from a pure diblock copolymer, increasing the swelling leads eventually to a disordered phase, a process that occurs via the gyroid and cylinder phases near the methanol-rich region, and via a direct lamellar to disordered transition near the THF-rich region. These trends agree well with the accepted tenet that addition of solvents effectively decreases χN and shifts the effective composition of the diblock copolymer towards the more selective solvent by inducing non-uniform swelling. Increasing solvent size leads to preferential swelling and at α=0.01, it results in depletion of PHEMA at the methanol-rich core of the PHEMA domains. Consequently, the cylinder and gyroid phases are stabilized for significantly larger regions of the phase diagram. Besides morphological control, co-solvent annealing also allows some control on domain size by tuning swelling factor and solvent ratio.

Based on the density distribution of the various components, the stability of cylinder and gyroid phases could be attributed to alleviation of packing frustration of the copolymer by the solvents, particularly methanol. Increasing χN also leads to the stabilization of these phases, although over the range of χN values studied this effect was milder than that of increasing solvent size. Since simulating high values of χN is computationally prohibitive, we proposed a combination of a somewhat higher α and lower χN than experiments to mimic the phase behavior at high χN, at least qualitatively. We observe a cylinder to gyroid to lamellar phase transition as the ratio of methanol:THF is increased over experimentally relevant swelling factors, although the location of the predicted phase boundaries does not exactly coincide with experiments. This limitation may be partially rooted on the errors associated with the estimation of χ values from solubility parameters; better estimates of the χ parameter should yield more accurate theoretical predictions. On the other hand, several sources of error may have also been at play in the experiments such as uncertainties on the molecular weights (and polydispersity) of the polymers, variation in the solvent composition, and the possible occurrence of long-lived metastable states.

Altogether, our theoretical calculations are consistent with the experimental finding that, starting with a 50:50 block copolymer, the gyroid phase can be stabilized by the swelling with a mixed solvent of a suitable composition. They also validate the general strategy of using a mixture of two solvents as a means to vary the solvent quality to allow access to different phases of interest even at a fixed temperature. Whether such a strategy could be used to target bicontinuous phases other than the gyroid remains to be explored but we suspect that non-symmetric block copolymer compositions could be more suitable and that at least one oligomeric "solvent" would be needed to more drastically alleviate the packing frustration that is typically associated with the lack of stability of such complex phases[38,39]. Our results also suggest some areas that need further improvement and investigation. A more atomistic approach or additional experimental data (for calibration) would be needed to

obtain more reliable χ parameters and overcome some of the limitations associated with the group-contribution methods that we adopted in this work. Also, more experimental and modelling work is needed to elucidate the pathways and kinetics rates associated with the formation of different phases and their inter-conversion.

Acknowledgements

This work was supported by Grant CBET 0756248 from the National Science Foundation. We are thankful to Prof. David Morse from University of Minnesota for the code for implementing SCFT. F.A.E. is grateful for computer cycles supplied by the Extreme Science and Engineering Discovery Environment, which is supported by National Science Foundation Grant No. OCI-1053575.

Appendix

1: Possibility of two-phase coexistence

The curvature of free energy (second derivative) with respect to volume fraction was calculated to detect multiphase coexistence. Two-phase coexistence occurs when the curvature of the free energy-volume fraction graph becomes negative, or contains an inflexion point[9]. The curvature is calculated from second-order central finite difference, i.e., $\frac{\partial^2 F}{\partial \varphi^2} = \frac{F(\varphi+\Delta\varphi)-2F(\varphi)+F(\varphi-\Delta\varphi)}{(\Delta\varphi)^2} + O((\Delta\varphi)^2)$. For all points studied, we did not observe a negative curvature although as α was increased the curvature became less positive. Figure A1 shows the free energy and curvature at χN=40, α=0.01 and swelling factor 5 where the curvature was least positive near 50:50 methanol:THF.

2: Normalized density distribution on increasing χN

Figure A2 shows the density distribution of all the components when increasing χN from 30 at the smallest solvent size. Two effects can be seen: first, the interface gets sharper as χN is increased. Second, the solvent distributes uniformly across both (PMMA-rich and PHEMA-rich) domains and its density variation (around the average) is only ~ 5%. This variation is much smaller than that observed upon increasing solvent size (as illustrated in Fig. 5).

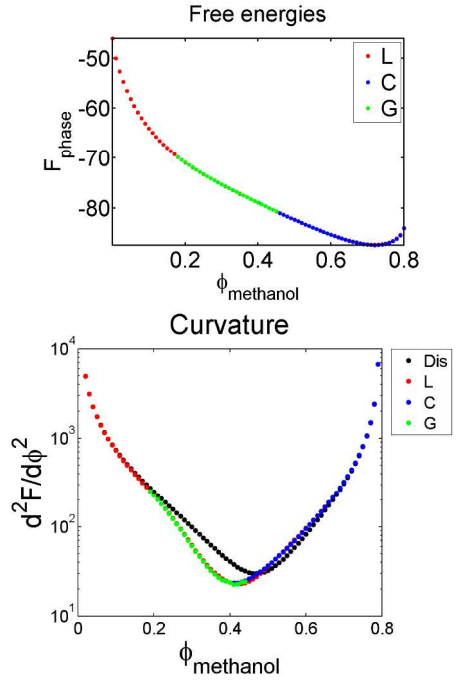

Figure A1: Free energy values and curvature at χN=40, α=0.01, swelling factor=5.

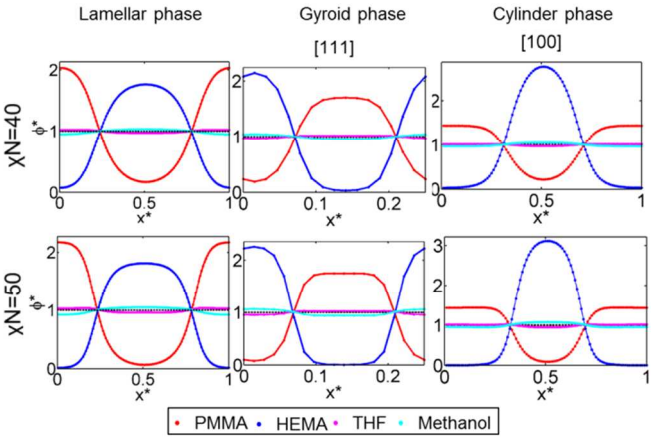

Figure A2: Effect of increasing χN on the density distributions of different components. Morphologies relevant to α=0.002, swelling factor = 3.3 with 80:20 methanol:THF (same as Figure 6). The lowest value of χN=30 is not shown here (disordered phase).

References

1 S. B. Darling, *Energy Environ. Sci.*, 2009, **2**, 1266.
2 A. S. Zalusky, R. Olayo-Valles, J. H. Wolf and M. A. Hillmyer, *J. Am. Chem. Soc.*, 2002, **124**, 12761.
3 A. Gabashvili, D. D. Medina, A. Gedanken and Y. Matsai, *J. Phys. Chem. B,* 2007, **111**, 11105.

4 M. Park, C. Harrison, P. M. Chaikin, R. A. Register and D. H. Adamson, *Science*, 2007, **276**, 1401.
5 K. J. Hanley and T. P. Lodge, *Macromolecules*, 2000, **33**, 5918.
6 P. Alexandridis, U. Olsson and B. Lindman, *Langmuir*, 1998, **14**, 2627.
7 E. W. Cochran, C. J. Garcia-Cervera and G. H. Fredrickson, *Macromolecules*, 2006, **39**, 2449.
8 D. A. Davidock, M. A. Hillmyer and T. P. Lodge, *Macromolecules*, 2003, **36**, 4682.
9 J. K. Bosworth, M. Y. Paik, R. Ruiz, E. L. Schwartz, J. Q. Huang, A. W. Ko, D.-M. Smilgies, C. T. Black and C. K. Ober, *ACS Nano*, 2008, **2**, 1396.
10 M. Y. Paik, J. K Bosworth, D.-M. Smilges, E.L. Schwartz, X. Andre and C. K. Ober, *Macromolecules*, 2010, **43**, 4253.
11 C. Sinturel, M. Vayer, M. Morris and M. A. Hillmyer, *Macromolecules*, 2013, **46**, 5399.
12 J. D. Cushen, L. Wan, G. Pandav, I. Mitra, G. E. Stein, V. Ganesan, R. Ruiz, C. G. Willson and C. J. Ellison, *J. Polym. Sci. Part B: Polym. Phys.*, 2014, **52**, 36.
13 T. Hashimoto, M. Shibayama and H. Kawai, *Macromolecules*, 1983, **16**, 1093.
14 J. R. Naughton and M. W. Matsen, *Macromolecules*, 2002, **35**, 5688.
15 C. Huang and T. P. Lodge, *Macromolecules*, 1998, **31**, 3556.
16 C. Huang, and Y. Hsu, *Phys. Rev. E*, 2006, **74**, 051802.
17 H. Jia, H. Huang, T. He and Y. Gong, *J. Chem. Phys.*, 2012, **137**, 224902.
18 Y. Chang, H. Hsueh, W. Chen and C. Huang, *Polymer*, 2005, **46**, 3942.
19 E. J. W. Crossland, M. Kamperman, M. Nedelcu, C. Ducati, U. Wiesner, D.-M. Smilgies, G. E. S. Toombes, M. A. Hillmyer, S. Ludwigs, U. Steiner and H. J. Snaith, *Nano Lett.*, 2009, **9**, 2807.
20 R. Maeda, M. Chavis, N. You and C. K. Ober, *J. Photopolym. Sci. Technol.*, 2012, **25**, 17.
21 M. Chavis, U. Wiesner, and C. K. Ober, *in preparation*. Also M. Chavis, Chapter 5 of Ph.D. Thesis at Cornell University, 2014, submitted.
22 M. W. Matsen and M. Schick, *Phys. Rev. Lett.*, 1994, **72**, 2660.
23 T. Suo, D. Yan, S. Yang and A.C. Shi, *Macromolecules*, 2009, **42**, 6791.
24 D. Morse, C. Tyler, A. Ranjan, J. Qin, R. Thiagarajan, see http://research.cems.umn.edu/morse/code/pscf/home.php (revision 11)
25 National Institute for Materials Science database: http://polymer.nims.go.jp/index_en.html
26 M. Rubinstein and R. H. Colby, Polymer physics, Oxford University Press, Oxford, New York, 2003.
27 M. I. Giannotti and G. J. Vansco, *ChemPhysChem*, 2007, **8**, 2290.
28 J. Brandrup, E. H. Immergrut, E. A. Grulke, *Polymer Handbook,* (John Wiley and Sons, 4th ed. 1999).
29 C. M. Hansen, *Hansen solubility parameters: a user's handbook* (CRC Press, Boca Raton, 2007).
30 D. W. vanKrevelen, *Properties of Polymers: their correlation with chemical structure, their numerical estimation and prediction from additive group contributions*, (Elsevier, Amsterdam, New York, 1990).
31 A. F. M. Barton, *CRC handbook of polymers-liquid interaction parameters and solubility)parameters*, (CRC Press, Boca Raton, 1990.
32 K. W. Gotrik, A. F. Hannon, J. G. Son, B. Keller, A. Alexander-Katz and C. A. Ross, *ACS Nano*, 2012, **6**, 8052.
33 J. Matous, A. Zivny and J. Biros. *Collect. Czech. Chem. Commun*. 1972, **37**, 3960. Also: www.ddbst.com/ddb.html
34 A. Ranjan, J. Qin and D. C. Morse, *Macromolecules*, 2008, **41**, 942.
35 M. W. Matsen, *Phys. Rev. Lett.*, 1998, **80**, 4470.
36 R. A. Wickham, A. C. Shi and Z. Wang, *J. Chem. Phys.*, 2003, **118**, 10293.
37 M. W. Matsen, *J. Chem. Phys.*, 2001, **114**, 8165.
38 F. Martinez-Veracoechea and F.A. Escobedo, *Macromolecules* 2009, **42**, 1775.
39 A. J. Meuler, M. A. Hillmyer and F. S. Bates, *Macromolecules*, 2009, **42**, 7221.

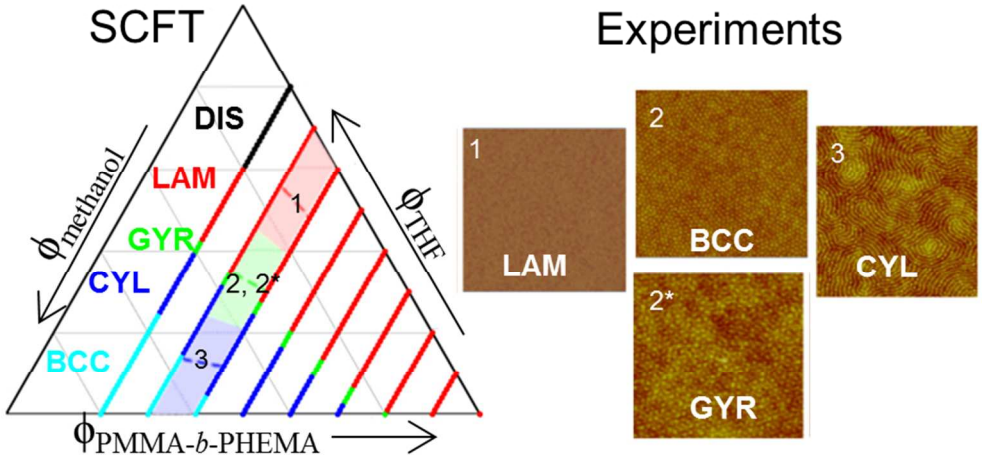

Self Consistent Field Theory predicts, consistent with experiments, that a symmetric block-copolymer forms a gyroid phase in a binary solvent